Nonlinear Resonance in Neuron Dynamics

Scott Rader, Diek W. Wheeler, W. C. Schieve, and Pranab Das*

Center for Studies in Statistical Mechanics and Complex Systems and Physics Department, The University of Texas, Austin, TX 78712

Z. Naturforsch. **50a**, 718–726 (1995); received May 9, 1994

Hübler's technique using aperiodic forces to drive nonlinear oscillators to resonance is analyzed. The oscillators being examined are effective neurons that model Hopfield neural networks. The method is shown to be valid under several different circumstances. It is verified through analysis of the power spectrum, force, resonance, and energy transfer of the system.

Key words: Nonlinear resonance, Hopfield model, two-neurons, slaving.

I. Introduction

In 1982, Hopfield introduced the dynamical neural network that is now referred to as the Hopfield neural network [1]. This was important for neural network research because it demonstrated how a network built from simple processing units, or neurons, could have emergent collective computational abilities. In particular, content-addressable memories, generalization, familiarity recognition, categorization, error correction, and time sequence retention become emergent collective properties of the Hopfield neural network. Since Hopfield's work in the early 1980's, there has been an explosion of research in the field of neural networks [2, 3].

The Hopfield neural network, as presented by Hopfield in 1982, is a system of neurons where each neuron can be in one of two states, $V=0$ or $V=1$. The system evolves through asynchronous updating of each neuron's state. A significant difference between this network and previously conceived networks is that a Hopfield network is fully interconnected with no specific input or output layer. The system starts in a certain state, which corresponds to some point in the phase space, and then evolves through time. Several years later, Hopfield extended his discrete neural system to a continuous, deterministic system described by one or more differential equations [4].

Schieve, Bulsara, and Davis [5] later developed the notion of *effective* neurons as a way to simplify the study of large Hopfield neural networks. The idea is based on Haken's slaving principle [6, 7], which describes the adiabatic elimination of fast-relaxing slave variables in favor of slow-varying master variables in solutions to the long time dynamics of a system. The properties of a chaotic attractor in a four neuron model, believed to be the simplest model of chaos in such a system, and the possible attracting states in a two-neuron system, have been evaluated [8, 9]. The numerical evidence for such "slaving" will be discussed later in this paper.

The effective neuron can be stimulated in such a way that a small driving force produces a large resonance response from the system. Nonlinear oscillators (neurons in this instance) have unique and subtle resonance conditions that differ from ordinary linear oscillators. A sinusoidal driving force can drive to resonance, or control, linear oscillators, but not nonlinear oscillators. Nonlinear oscillators have a frequency-amplitude coupling, where the frequency always changes if the amplitude changes. This coupling makes it difficult for a sinusoidal driving force to drive a nonlinear oscillator to resonance, so a more complex force, such as the one suggested by Hübler [10, 11], is required.

The method for bringing a nonlinear system to resonance requires finding an aperiodic driving force that matches at all times the frequency and phase of the system. This is accomplished by calculating the *time-reflected* transient dynamics of the unperturbed nonlinear system. For example, picture a particle in a potential well, where the system is slightly damped. If the particle starts in a highly stimulated state, it eventually comes to rest at the bottom of the well. The particle's frequency in the stimulated state is large, and decreases until the particle comes to rest. Knowing

* Present address: Elon College, Physics Department, 2236 Campus Box, Elon College, NC 27244, USA.

Reprint requests to Prof. W. C. Schieve.

0932-0784 / 95 / 0800-0718 $ 06.00 © – Verlag der Zeitschrift für Naturforschung, D-72027 Tübingen

this motion, the unperturbed dynamics can be reflected in time. By applying a force matching the time-reflected dynamics to a particle at rest, a particle can be placed immediately into a state of resonance.

There are three types of resonance that are a result of the methods used in solving for the resonant forces. In each case, some quantity of the system is optimized given certain constraints on the system. Since the optimizations and constraints are not the same in all three cases, differing resonant forces result. Strong resonance, which is discussed in Section III, is characterized by a force calculated from the time-reflected dynamics that perfectly mirror the unperturbed dynamics of the system. When the time-reflected dynamics vary slightly from the unperturbed dynamics, the force is in medium resonance with the system. If there is a large difference between the unperturbed and time-reflected dynamics, then a state of weak resonance is achieved. The objective here is to numerically investigate such resonant forces in a slaved neural network. Haken's slaving principle as it applies to effective neurons is explored in more detail in Section II. Section III describes the notion of optimal resonance driving. Presented in Sect. IV are numerical results supporting the validity of slaving for a driven system. Section V will conclude with simulation results and a discussion of what was learned.

II. Haken's Slaving Principle and Effective Neurons

Haken introduced the slaving principle [6, 7] to reduce the dynamics of large complex systems into low dimensional subsets that might be easier to analyze. This principle is used extensively in statistical physics and quantum optics. System variables are divided between those that evolve quickly to a steady-state and those that evolve more slowly. The fast-relaxing variables follow the slow-relaxing master variables. The "slaved" variables are adiabatically eliminated leaving a lower dimensional system consisting of just the remaining master variables.

The principle can be applied to large neural networks where the computational cost can become excessive and where a qualitative understanding of the dynamics might be achieved. The slaved neurons are driven by the master neurons of the network. The master neuron may be as simple as a single neuron. Schieve, Bulsara, and Davis [5] introduced the idea of effective neurons and applied the notion to Hopfield's deterministic network model [4],

$$M_i \ddot{U}_i + C_i \dot{U}_i + U_i/R_i = \sum_{j \neq i=1}^{N} J_{ij} \tanh(U_j). \quad (1)$$

Here U_i is the potential of the ith neuron, M_i is the inductance, C_i is the capacitance, R_i is the membrane resistance, and J_{ij} are the symmetric connection weights. The inductive term was introduced by Babcock and Westervelt [12] to model the transient response between neurons.

Two assumptions must be made for the effective neuron approximation to be valid. First, the membrane resistances for the slaved neurons, R_i, must be much smaller than the resistance for the master neuron, R_1 ($R_i \ll R_1$, $i \neq 1$). This allows the slaved neurons to reach their steady-state faster than the master neuron. Second, the inductance of the slaved neurons (M_i, $i \neq 1$) must be small to prevent oscillations from developing that might keep the slaved neurons from ever reaching a time independent steady-state.

With the above two provisions, it can now be assumed that

$$C_i \dot{U}_i \approx 0 = -U_i/R_i + \sum_{j \neq i=1}^{N} J_{ij} \tanh(U_j) \; (i \neq 1) \quad (2)$$

for all of the slaved neurons. For simplicity, one can make the approximation $\tanh(x) \approx x$ for small x, which leads to the final equation for an effective neuron ($i=1$),

$$M_1 \ddot{U}_1 + C_1 \dot{U}_1 + U_1/R_1 = J_{11} \tanh(U_1), \quad (3)$$

where a self-connection term not present in (1) is

$$J_{11} = \sum_{j=2}^{N} J_{1j}^2 R_j > 0. \quad (4)$$

Here an effective self-coupling constant J_{11} now appears which depends on the J_{1j} ($j \neq 1$).

With the presence of an external driving term, a similar but slightly more complicated effective neuron formulation may be derived for a Hopfield neural network [13]. Assume an external driving force of the form

$$F_i(t) = A_i \cos(\omega_i t). \quad (5)$$

The activity of the master neuron can now be described by the equation

$$M_1 \ddot{U}_1 + C_1 \dot{U}_1 + U_1/R_1 = \sum_{i=2}^{N} J_{1i} \tanh(U_i) + A_1 \cos(\omega_1 t). \quad (6)$$

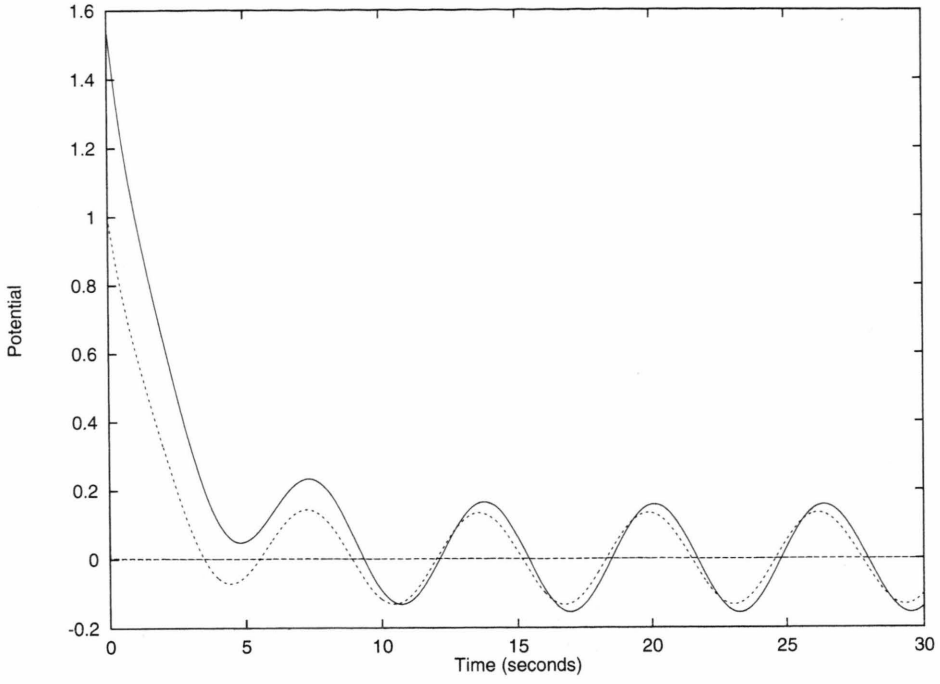

Fig. 1. Real vs. Single Effective Neuron Dynamics. The potential versus time of a 256 dimensional neural network and its corresponding single effective neuron. The effective neuron (dotted line) closely models the master neuron (solid line). The slaved neurons fluctuate around zero potential. $J=1$, $R=1.56\times10^{-3}$, $A_1=0.1$, $A_2=0.1$, $\omega_1=1$, $\omega_2=1$.

The slaved neurons are governed by the equations

$$C_i\dot{U}_i = -U_i/R_i + \sum_{j\neq i=1}^{N} J_{ij}\tanh(U_j) + A_i\cos(\omega_i t) \quad (i=2\ldots N). \tag{7}$$

To solve (7), one can assume a solution of the form (Gardiner [7])

$$U_i = \int_{-\infty}^{t} \mathrm{d}\tau e^{-(t-\tau)/R_i} \cdot\left(\sum_{j\neq i=1}^{N} J_{ij}\tanh(U_j(\tau)) + A_i\cos(\omega_i\tau)\right). \tag{8}$$

The first term of the integral can be integrated by parts to yield

$$\sum_{j\neq i=1}^{N}\left[J_{ij}R_i\tanh(U_j(t)) - J_{ij}R_i\int_{-\infty}^{t} e^{-(t-\tau)/R_i}\operatorname{sech}^2(U_j(\tau))\,\dot{U}_j(\tau)\,\mathrm{d}\tau\right]. \tag{9}$$

Since $R_i \ll 1$ in the exponential, the second term in (9) can be set to zero. Integration of the second term in (8) results in

$$D_i \equiv \frac{A_i R_i}{1+R_i^2\omega_i^2}[\cos(\omega_i t) + R_i\omega_i\sin(\omega_i t)] \quad (i=2\ldots N). \tag{10}$$

Equations (9) and (10) can be combined into a solution for U_i, which, when applied twice to (6), results in an effective neuron equation with an external driving force,

$$M_1\ddot{U}_1 + C_1\dot{U}_1 + U_1/R_1 = \sum_{i=2}^{N} J_{1i} \cdot\tanh\left[J_{i1}R_i\tanh(U_1) + \sum_{j\neq i=2}^{N} J_{ij}R_i \cdot\tanh\left(\sum_{k\neq j=1}^{N} J_{jk}R_j\tanh(U_k) + D_j\right) + D_i\right] + A_1\cos(\omega_1 t). \tag{11}$$

Figures 1–5 show examples of an effective neuron that models one master neuron and 255 slaved neurons. Since all of the slaved neurons are identical ($J_{ij}=J$, $R_i=R$), they are represented in the graphs by a single line that barely oscillates about the zero potential. The effective neuron can be seen to model the master neuron fairly closely in Figure 1. Manipulation

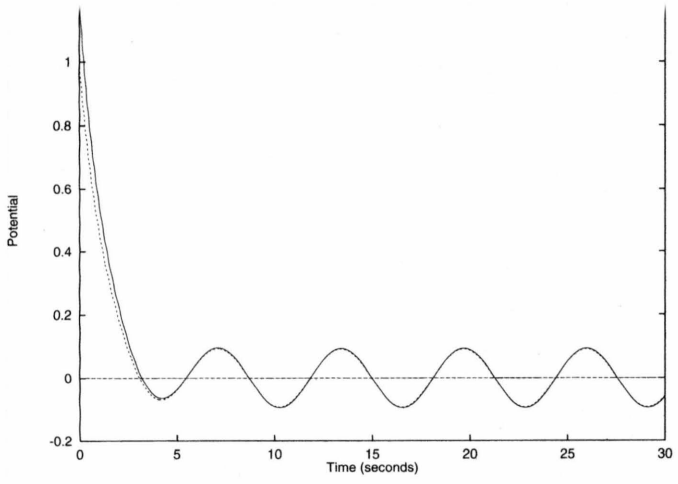

Fig. 2. Real vs. Single Effective Neuron Dynamics. The potential versus time of a 256 dimensional neural network and its corresponding single effective neuron. As J is decreased, the agreement between the effective neuron (dotted line) and the master neuron (solid line) becomes better. The slaved neurons fluctuate around zero potential. $J=0.5$, $R=1.56\times10^{-3}$, $A_1=0.1$, $A_2=0.1$, $\omega_1=1$, $\omega_2=1$.

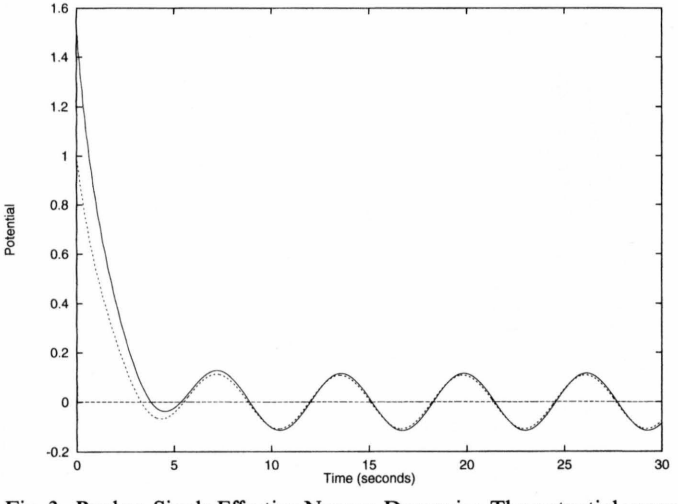

Fig. 3. Real vs. Single Effective Neuron Dynamics. The potential versus time of a 256 dimensional neural network and its corresponding single effective neuron. As R is decreased, the agreement between the effective neuron (dotted line) and the master neuron (solid line) becomes better. The slaved neurons fluctuate around zero potential. $J=1$, $R=1.04\times10^{-3}$, $A_1=0.1$, $A_2=0.1$, $\omega_1=1$, $\omega_2=1$.

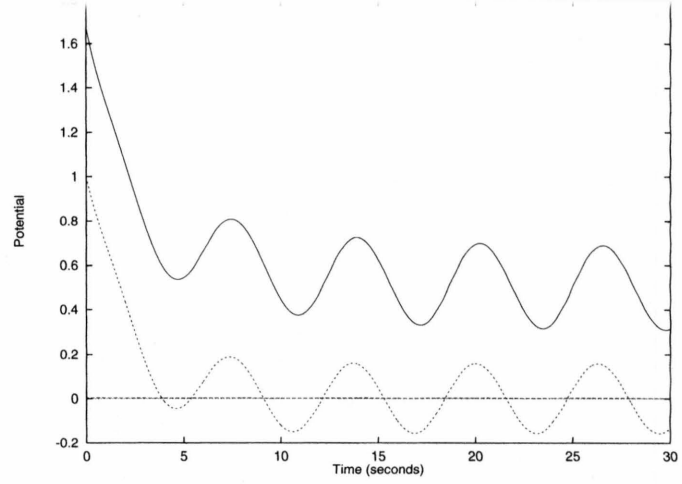

Fig. 4. Real vs. Single Effective Neuron Dynamics. The potential versus time of a 256 dimensional neural network and its corresponding single effective neuron. If J is too large, the effective neuron (dotted line) fails to properly model the master neuron (solid line). The slaved neurons fluctuate around zero potential. $J=1.2$, $R=1.56\times10^{-3}$, $A_1=0.1$, $A_2=0.1$, $\omega_1=1$, $\omega_2=1$.

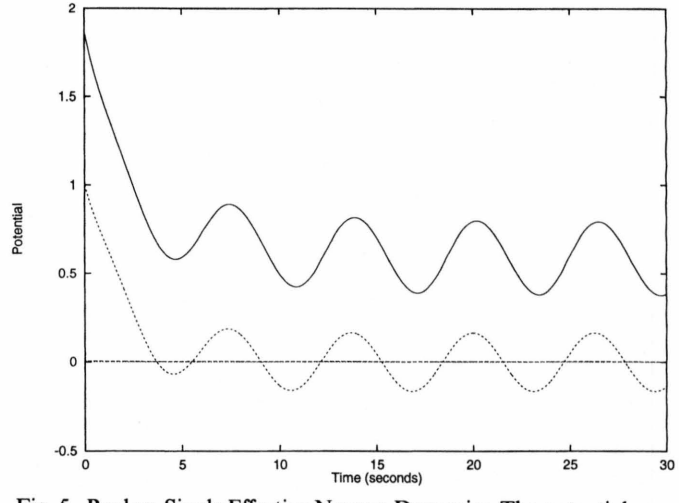

Fig. 5. Real vs. Single Effective Neuron Dynamics. The potential versus time of a 256 dimensional neural network and its corresponding single effective neuron. If R is too large, the effective neuron (dotted line) fails to properly model the master neuron (solid line). The slaved neurons fluctuate around zero potential. $J=1$, $R=2.08\times10^{-3}$, $A_1=0.1$, $A_2=0.1$, $\omega_1=1$, $\omega_2=1$.

of the parameters J and R can lead to better or worse fits between the master and effective neurons. Figures 2 and 3 demonstrate how lowering the values of J and R can increase the correlation between the effective and master neurons. An increase in J and R (Figs. 4 and 5) results in poor modeling behavior by the effective neuron. In order to maintain a consistent fit between the effective and master neurons as the number of neurons increases, the expression $NJR=\alpha$ must remain relatively constant. That is, as the number of neurons N increases, so must either J or R similarly decrease in order to maintain the slaving.

Equation (11) can be simplified by removing the driving forces from the slaved neurons. This leaves a driving force on only the master neuron. Further simplifications can be made to (11) by taking first order approximations to the tanh terms due to the small size of the $J_{ij}R_i$ factors. The resulting effective neuron equation to lowest order in J_{ij} and R_i is

$$M_1\ddot{U}_1 + C_1\dot{U}_1 + U_1/R_1 = J_{11}\tanh(U_1) + A_1\cos(\omega_1 t). \tag{12}$$

It is this equation that will be used in following sections.

III. Optimal Resoncance Driving

The strong resonance case represents optimal resonance driving of a nonlinear system (Hübler [10]). Consider first the damped, driven nonlinear oscillator,

$$m\ddot{x} + \eta\dot{x} + \frac{\partial V(x)}{\partial x} = F(t), \tag{13}$$

where η is the damping constant and $F(t)$ is the optimal driving force to be determined. To calculate the optimal driving force, a Lagrangian is constructed to minimize the mean square average of the driving force (the fluctuation),

$$\bar{F}^2 = \int_0^{T(\Delta H)} |F(t)|^2\,dt. \tag{14}$$

There are two constraints on the Lagrangian. One is (13), and the other is that the energy transfer into the oscillator is fixed over a set of periods of time T. The energy transfer is

$$\Delta H = \int_0^{T(\Delta H)} F\dot{x} - \eta\dot{x}\,dt = \text{fixed}, \tag{15}$$

where the constraint on the energy H is given by

$$H = \frac{m}{2}\dot{x}^2 + V(x). \tag{16}$$

With the above constraints, a Lagrangian

$$L = |F(t)|^2 - \mu(t)\left(m\ddot{x} + \eta\dot{x} + \frac{\partial V(x)}{\partial x} - F(t)\right) - \lambda\left(\frac{m}{2}\dot{x}^2 + V(x) - H\right)\delta_D(t-T) \tag{17}$$

is obtained (Wargitsch and Hübler [14]). Note that in this variational problem T depends on ΔH, and some subtlety must be employed (Akhiezer [15]).

The optimal driving force is

$$F(t) = 2\eta\dot{y}. \tag{18}$$

Here y is a solution to

$$\ddot{y} - \eta\dot{y} + \frac{\partial V}{\partial y} = 0. \tag{19}$$

Equation (19) is the time-reflected (13) with zero force. This is Hübler's intuitive idea for the goal dynamics with an implicit driving force.

The optimal driving force $F(t)$ above will now be substituted for the sinusoidal driving force in (12). The main object of this section of the paper is to investigate the resonance inherent in the following equations under optimal driving:

$$\ddot{U} + \eta\dot{U} + U - \tanh(U) = F(t), \tag{20}$$

$$\ddot{U} - \eta\dot{U} + U - \tanh(U) = 0, \tag{21}$$

$$F(t) = 2\eta\dot{U}. \tag{22}$$

Labeling subscripts have been dropped, and from now on the membrane resistance, the inductive inertial mass, and the self-connection term will be set to one. Equations (20)–(22) are investigated numerically in the next section.

Previously [10], Hübler numerically investigated optimal driving of the pendulum described by

$$\theta\ddot{y} + \eta_1\dot{y} + c_1 y + c_2\sin(y) = F(t). \tag{23}$$

There it was shown that despite the presence of many vibrational modes in the system, only the base frequency of the system was stimulated. All of the higher modes remained unexcited. Further numerical results (Wargitsch and Hübler [14]) show how the effectiveness of optimal driving increases with nonlinearity in P for

$$\ddot{x} + \eta\dot{x} + x + x^{p-1} = F(t). \tag{24}$$

IV. Numerical Evidence for Slaving in Driven Systems

The main point of this section is to numerically demonstrate the presence of nonlinear resonance in the equations derived at the end of the previous section. Equations (20)–(22) can now be examined to see if they in fact represent optimal resonance driving of a slaved neural system, as discussed in Section II.

After first analytically solving (20, 21) is solved numerically and yields the plot of the potential U versus time in Figure 6. The neuron's potential grows exponentially in time, verifying that there is a resonance in the neuron. A calculation of the power in the system shows that it is always greater than zero, and that the energy always transfers in one direction, from the forcing action $F(t)$ in (22), to the neuron. This is shown in Figure 7.

A check must be made to see that the system is not being overdriven. The driving force must be smaller than, or equal to the magnitude of the sum of the other forces present in the system. If the forcing term is at all times much greater than the other forces in the system, then the system effectively is overdriven, and it will not show resonance. Figure 8 shows a plot of the driving force versus the potential and frictional forces in the system. The driving force is clearly smaller than the other forces.

Another important consideration in this analysis is whether this potential is far from zero, or close to zero. If $|U| \gg 0$, then $\tanh(U) \approx 1$. If a change of variable is now performed ($W = U - 1$), one obtains

$$\ddot{W} + \eta \dot{W} + W = F(t), \tag{25}$$

an equation for a damped, driven harmonic oscillator. If $U \ll 1$, then $\tanh(U) \approx U$, and (20) becomes

$$\ddot{U} + \eta \dot{U} = F(t). \tag{26}$$

Equations (25) and (26) show that the nonlinear effects due to $\tanh(U)$ are only important for an intermediate range of potentials. The dotted vertical lines in Fig. 6 delineate the times when the nonlinearity has the greatest effect. Between 350 and 500 seconds, the system maintains a potential between 0.5 and 3.0 at least fifty percent of the time. In this limited potential range, the amplitude of the potential has not yet grown enough to saturate the tanh term.

To better understand the mechanisms behind the resonance, the frequencies present in the time-reflected dynamics of (21) are calculated. Figure 9 shows a graph of the power spectral density plotted versus frequency for several different time segments. The two lower peaks show that the power peak is changing the frequency. During the times when the system is affected most by the nonlinearity in the tanh term (~ 350–500 sec), as delineated in Fig. 6, nonlinear behavior analogous to entrainment (Minorsky [16]) begins to take place, eventually settling into the frequency exhibited by the topmost peak. Here the oscillator entrains the effective frequency of the nonlinear driving force, (22). This by construction is $\omega = 1$. The transient nature of the nonlinear regime allows only finite time segments to be sampled, resulting in the jagged appearance of the plots in Figure 9.

V. Numerical Investigation of Optimal Resonance

By moving the effective neuron system off optimal resonance, the medium and weak resonance cases may be explored. Since ΔH is an action integral, it should have a maximum under a variation of the system in configuration space. To adjust for optimum conditions, a constant factor, K, is inserted into the linear term in (20). The new equation is

$$\ddot{U} + \eta \dot{U} + K U - \tanh(U) = F(t), \tag{27}$$

where $F(t)$ is the resonance condition from (22), and $\dot{U}$ is obtained from (21). The plots of ΔH versus K in Fig. 10 exhibit a sharp peak at $K = 1$. The bottom plot begins at $K = 1$ since there is a loss of energy from the system at values of K smaller than one. This energy loss arises when the system is in the middle of the nonlinear regime delineated in Figure 6. During entrainment some oscillations may be dying out as others are beginning to grow, which may result in a net loss of energy for the system. The apparent dip at $K = 2.5$ is exaggerated due to the logarithmic scaling of the plot. The upper two peaks demonstrate how the energy absorption continues to grow once the entrainment has ended.

The three-dimensional plots in Figs. 11–13 show how changing η in (27) also affects the resonance of the system. Figure 11 shows that variations in η have little effect on the system near the start of the nonlinear regime. In Figs. 12–13, a variation of η only seems to have an effect when the system is at resonance close to $K = 1$. An increase in η causes a slight decrease in energy absorption for the system. A decrease in η leads to an increase in system energy. The smaller η is, the

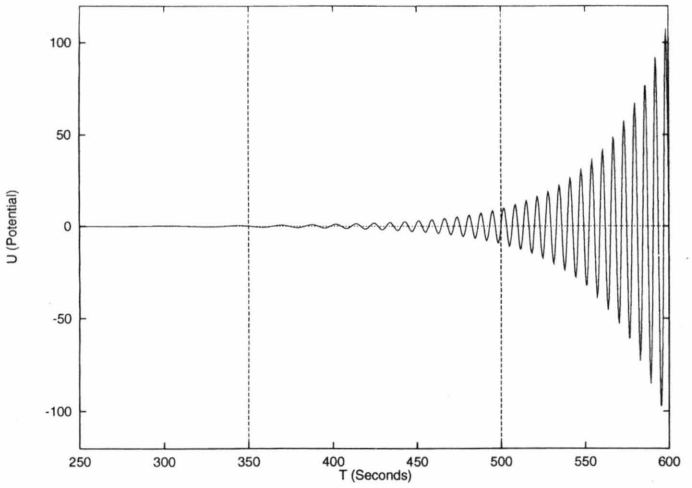

Fig. 6. Single Neuron Dynamics. The potential versus time for an optimally driven effective neuron. The neuron's potential is resonating, and energy is continuously being fed into the neuron, so the neuron's potential will grow. The region between the dotted vertical lines is where the nonlinearity of the system is greatest. $\eta = 0.05$.

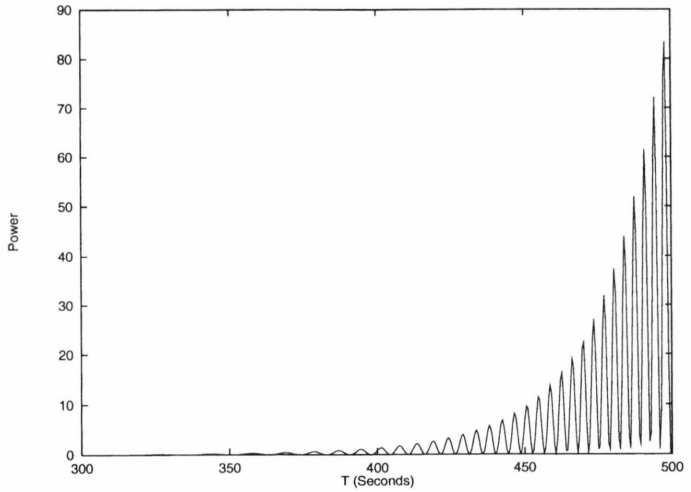

Fig. 7. Single Neuron Energy Transfer. Since the power is always greater than zero and increasing, the energy is transferred from the driving force to the neuron. This is a condition for optimal resonance. $\eta = 0.05$.

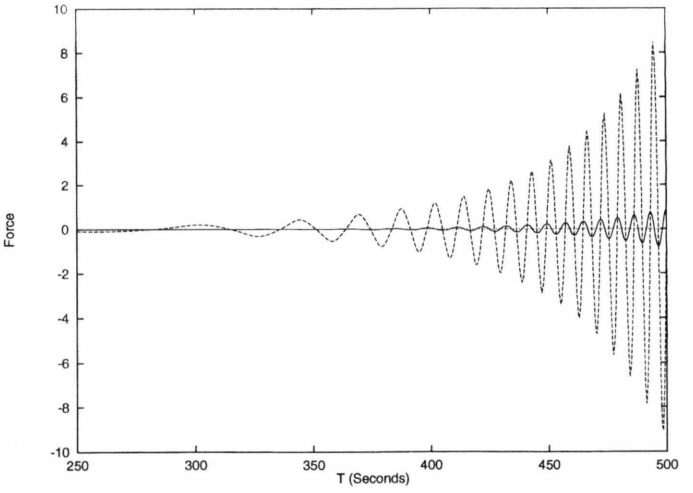

Fig. 8. Single Neuron Comparison of Forces. A comparison over time of the forces present in the system. The solid line is the driving force, and the dotted line is the frictional force plus the force due to the potential. Here, the driving force is clearly smaller than the "undriven" forces, which indicates that the system is not being overdriven.

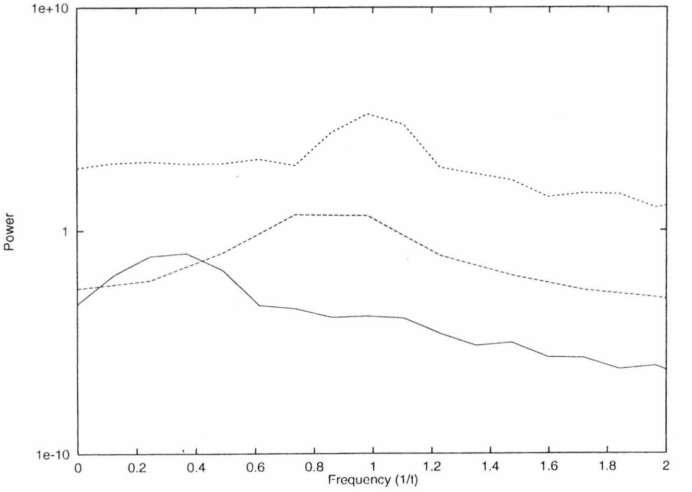

Fig. 9. Single Neuron Power Spectrum. For intermediate times ($\sim$350–500 sec), the power peak frequency can be seen to shift until it is fully entrained to the $\omega = 1.0$ frequency of the driving force. For long time dynamics (>500 sec), the power peak continues to grow in amplitude, indicating that the system has reduced to the analogue of a damped, harmonic oscillator being driven by a sinusoidally varying force. Temporal sampling from bottom to top: 326.0–377.2 seconds, 447.0–472.6 seconds, 630.0–681.2 seconds.

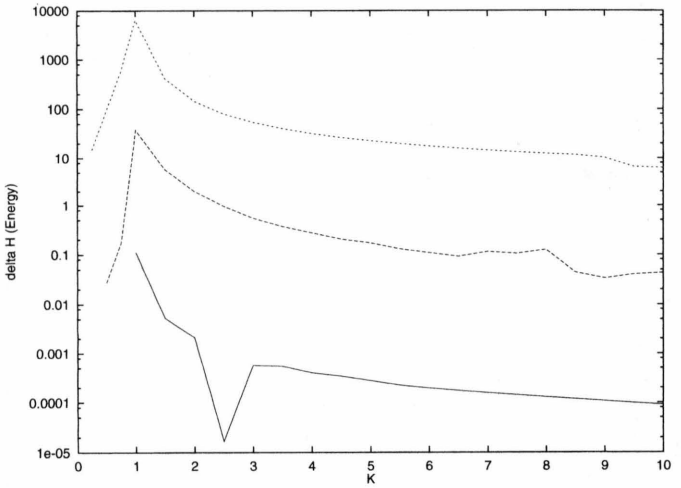

Fig. 10. Single Neuron Energy Resonance. This graph shows ΔH versus K. K is analogous to the square of the angular frequency in a harmonic oscillator. By varying K, a resonance curve is produced. When $K=1$, the maximum amount of energy is transferred from the driving force to the neuron. From bottom to top: Time = 400.0 seconds, Time = 500.0 seconds, Time = 600.0 seconds.

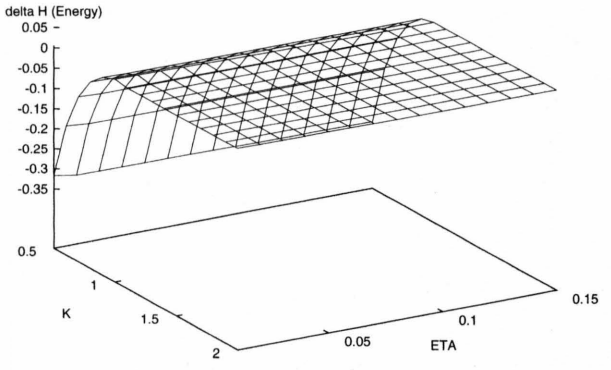

Fig. 11. Single Neuron Energy Resonance. This graph shows ΔH versus K and η. At the start of the nonlinear regime there is little variation with respect to η. Time = 350.0 seconds.

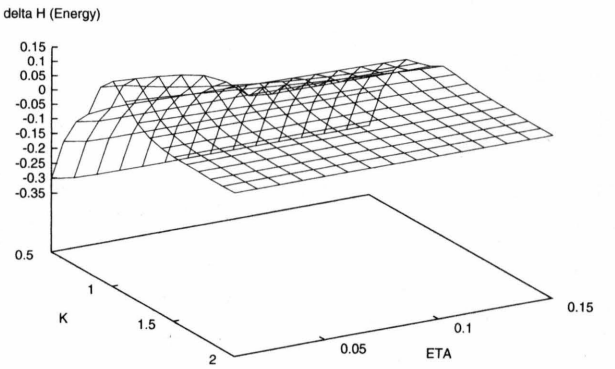

Fig. 12. Single Neuron Energy Resonance. This graph shows ΔH versus K and η. In the middle of the nonlinear regime, variations in η begin to appear only when $K=1$. As η decreases, energy increases since the frictional losses are decreased. Time = 400.0 seconds.

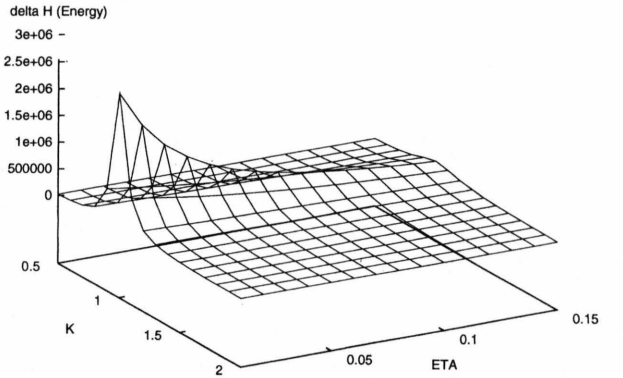

Fig. 13. Single Neuron Energy Resonance. This graph shows ΔH versus K and η. Outside the nonlinear regime, variations in η appear only when $K=1$. As η decreases, energy increases since the frictional losses are decreased. Time = 700.0 second.

less frictional losses there are, so the system tends to gain energy.

An effective Hopfield neuron with an added inertial term shows a clear resonance behavior when driven optimally, as discussed in Section III. Since a nonlinear system has a frequency-amplitude coupling, a sinusoidal driving force is not able to match the characteristic resonant frequencies inherent in the system. The application of Hübler's optimal resonance technique, however, does drive an effective neuron to resonance. At resonance, the system is not overdriven, and the transfer of energy is always from the driving force to the neuron. An analysis of the power spectrum shows that only a single base frequency ($\omega = 1$) is excited in the system, leaving all of the higher frequencies dormant. Therefore, in the long time evolution of the neural system, the optimal resonance force behaves analogous to a simple sinusoidal driving force for a linear oscillator. To drive the nonlinear system to optimal resonance, a force is used which depends on the nonlinear system's (time-reflected) internal dynamics, given by $F = 2\eta \dot{U}$.

Acknowledgement

W. C. Schieve would like to thank Alfred Hübler and Christoph Wargitsch for their discussions during his visits to the Beckman Institute (Chapman-Urbana, Illinois) and to Keio University (Yokohama, Japan).

[1] J. Hopfield, Proc. Natl. Acad. Sci. **79,** 2554 (1982).
[2] D. Amit, Modeling Brain Function, Cambridge University Press, Cambridge 1989.
[3] B. Müller and J. Reinhardt, Neural Networks, Springer-Verlag, Berlin 1990.
[4] J. Hopfield, Proc. Natl. Acad. Sci. **81,** 3088 (1984).
[5] W. C. Schieve, A. R. Bulsara, and G. M. Davis, Phys. Rev. A **43,** 2613 (1991).
[6] H. Haken, Synergetics, Springer-Verlag, Berlin 1977. Also: Advanced Synergetics, Springer-Verlag, Berlin 1993.
[7] C. Gardiner, Handbook of Stochastic Methods, Springer-Verlag, Berlin 1983.
[8] P. K. Das, W. C. Schieve, and Zhaojue Zeng, Physics Letters A **161,** 60 (1991).
[9] Zeng, Zhaojue, W. C. Schieve, and P. K. Das, Physica D **67,** 224 (1993).
[10] A. Hübler, Modeling and Control of Complex Systems; Paradigms and Applications, Modeling Complex Phenomena, edited by L. Lam, Springer, New York 1992. See also Ref. [14].
[11] A. Hübler and E. Lüscher, Naturwiss. **76,** 67 (1989); A. Hübler, Helv. Physica Acta **62,** 543 (1989); G. Reiser, A. Hübler, and E. Lüscher, Z. Naturforsch **42a,** 803 (1987).
[12] K. Babcock and R. Westervelt, Physica D **28,** 305 (1987).
[13] S. Rader, The Driven Hopfield Neural Network: Slaving and Resonance, M.S. thesis, Dept. of Physics, Univ. of Texas at Austin, 1993.
[14] C. Wargitsch and A. Hübler, Phys. Rev. E, to appear 1995.
[15] N. I. Akhiezer, The Calculus of Variations, Blaisdell, New York 1962.
[16] N. Minorsky, Introduction to Non-Linear Mechanics, J. W. Edwards, Ann Arbor 1947, Chapt. XVIII.